ISSN 1819-7140, Russian Journal of Pacific Geology, 2017, Vol. 11, No. 2, pp. 110–122. © Pleiades Publishing, Ltd., 2017.
Original Russian Text © V.V. Golozubov, N.N. Kruk, V.I. Kiselyov, S.N. Rudnev, S.A. Kasatkin, E.A. Kruk, 2017, published in Tikhookeanskaya Geologiya, 2017, Vol. 36, No. 2, pp. 44–57.

First Evidence for the Middle Triassic Volcanism in South Primorye

V. V. Golozubov[a, *], N. N. Kruk[a, c, **], V. I. Kiselyov[a], S. N. Rudnev[b], S. A. Kasatkin[a], and E. A. Kruk[b]

[a] *Far East Geological Institute, Far East Branch, Russian Academy of Sciences, pr. Stoletiya Vladivostoka 159, Vladivostok, 690022 Russia*

[b] *Sobolev Institute of Geology and Mineralogy, Siberian Branch, Russian Academy of Sciences (IGM SB RAS), pr. akademika Koptyuga 3, Novosibirsk, 630090 Russia*

[c] *Novosibirsk State University, ul. Pirogova 2, Novosibirsk, 630090 Russia*

**e-mail: golozubov@fegi.ru*

***e-mail: kruk@igm.nsc.ru*

Received February 5, 2016

Abstract—A detailed study of a relatively well-exposed fragment of the Barabash Formation in the southern part of the Voznesenka terrane is carried out to specify the geodynamic settings of the Permian volcanogenic and volcanogenic-sedimentary complexes in South Primorye. It is established that the basaltic flows juxtaposed in the studied sequence originated from sharply different sources. The geochemical characteristics indicate that the basalts from the sequence base were presumably derived by melting of oceanic lithospheric mantle or asthenosphere, while the source of the overlying basalts was lithospheric mantle reworked by a subduction process. The basalts are subsequently overlain by tuffaceous–terrigenous and terrigenous rocks and limestones with remains of Capitanian (Middle Permian) fauna. Accessory zircons extracted from the tuffaceous–terrigenous rocks yield an U–Pb concordant age of 233.3 ± 3.3 Ma (Middle Triassic Ladinian Stage) for the youngest zircon population. The obtained data lead us to conclude that the Barabash Formation is a tectonostratigraphic rather than stratigraphic unit and may be a fragment of the Triassic accretionary wedge. The obtained data cast doubt on the accepted assignment of this unit to the Voznesenka terrane. It is more logical to include it in the Laoelin–Grodekov terrane, which represents a fragment of the Late Paleozoic active continental margin. This suggests that the boundary between these blocks should be specified and the timing of the final stage of amalgamation of the Laoelin–Grodekov terrane with the terranes of the Bureya–Khanka orogenic belt should be revised.

Keywords: geodynamic settings, volcanism, geochemistry, U–Pb zircon dating, tectonic zoning, South Primorye

DOI: 10.1134/S1819714017020038

INTRODUCTION

South Primorye consists of two large lithotectonic domains of different ages: the linear Mesozoic Sikhote Alin folded systems formed during the evolution of the Pacific mobile belt and the Late Precambrian–Paleozoic terrane collage related to the evolution of the Central Asian Orogenic Belt (CAOB).

The Permian–Triassic transition is the key period in the evolution of the eastern CAOB. Some researchers believe that this time was marked by the collision of the Precambrian and Paleozoic blocks and the final formation of the pre-Mesozoic geological structure of the region.

The events that predated this transition are thought to be related to the evolution of the active margin of the Solonker paleoocean [2, 11]. These processes are marked by the formation of accretionary wedges with fragments of ophiolite sequences in the adjacent territories of China and Korea, and by the Early and Middle Permian volcanism followed by Permian intense deformations and abundant granite formation in Russian South Primorye [2, 6, 9]. In the Triassic, most of South Primorye was spanned by shallow-water marine sedimentation with no traces of endogenic activity. It should be noted that the first results of geochemical study of the Permian volcanic rocks [7] suggest a more complex geological evolution, but are consistent with the marginal continental setting related to the interaction of oceanic and continental plates in this region.

In Russian South Primorye, the most intense manifestation of Permian volcanism occurred in the Early Paleozoic terranes of the Bureya–Khanka orogenic belt and the Late Paleozoic Laoelin–Grodekov ter-

rane (Fig. 1). Early Permian volcanic rocks were found in the local exposures of the Dunai Formation (Sakmarian–Artinskian stages) in the Sergeevka terrane and the Kazachkinskaya Formation (Bolorian Stage) in the Laoelin–Grodekov terrane. The volcanic rocks of the Vladivostok Formation dated by the Middle Permian Wordian stage are more abundant. They are overlain by the Barabash Formation (and its age analogue, the tuffogenic–carbonate Chandalaz Formation), the age of which is determined as Capitanian on the basis of numerous faunal finds, mainly in limestones (foraminifers *Monodiexodina wanneri* (Schubert), *Skinnerella schucheryi* Dunb et Skinn.; pearworts *Dyscritella bogatensis* Kis., *Girtypora regula* Kis., brachyopods *Anidanthus ussuricus* (Frcsk), *Haydenella kiangsiensis* (Kays.)). According to [4], most of the sequences of the Barabash Formation are subdivided into two subformations: the lower subformation consisting mainly of basalts, volcanosedimentary rocks, and carbonates, and the upper subformation made up mainly of lavas and pyroclastic rocks of intermediate–felsic composition, as well as sedimentary rocks. These formations are characterized by a tight association of volcanic, volcanosedimentary, and sedimentary rocks, a gradual increase in the SiO_2 content in the volcanic products (from basalts and andesites to rhyolites) from the bottom upward, as well as coastal–marine and lagoonal sedimentation environments. The Barabash Formation, like other Permian formations, is deformed and intruded by mainly Late Permian granitoid intrusions (including the Gamov and Sedanka complexes) exhumed during subsequent erosion and overlain by Triassic rocks, which, correspondingly, form the upper structural stage.

The Triassic deposits in the southern part of the Voznesenka terrane are represented by a thick (over 1500 m) sequence of terrigenous rocks, which were accumulated in coastal–marine and more rarely lagoonal–continental environments during practically the entire period (from the Indian to the Norian, inclusive). The only exception is the western part adjacent to the Laoelin–Grodekov terrane (including the studied area), where the basal beds are dated to the Carnian stage while the Lower and Middle Triassic sediments are absent. Carnian floral assemblage was also identified in the Tal'min volcanosedimentary sequence in the northern part of the Laoelin–Grodekov terrane [4, 5].

It should be noted that no "direct" isotope datings are available for the volcanic rocks of the aforementioned stratotones: all of the available age determinations are based only on the finds of faunal remains in the terrigenous rocks associated with the volcanic rocks in the sequences. Due to the poor exposure, multiple tectonic reworking, and insufficient knowledge of the relationships between the beds even in the reference sequences, many questions concerning rock succession, true thickness, and degree of lateral persistence remain unclear. The insufficient geochemical study of the volcanic rocks makes it impossible to determine the geodynamic setting of this area in the Permian and Triassic. To solve at least some of the aforementioned problems, we carried out a detailed complex study of the relatively well-exposed section of the Barabash Formation in the southern part of the Voznesenka terrane. The results of these studies are presented below.

GEOLOGICAL POSITION

The studied sequence is situated on the left bank of the Barabashevka River, approximately 3 km northwest of the Barabash settlement. The sequence is oriented from the northwest to the southeast, practically across the strike of the sediments. The beds dip steadily to the southeast at angles of 40–50%. Immediately in the Barabashevka River valley, the base of the section is overlain by Cretaceous carbonaceous deposits; to the west, the volcanosedimentary sequences conformably rest (according to [3]) on the Middle Permian rocks of the Vladivostok Formation. From the top, the volcanosedimentary sequences are unconformably overlain by faunally characterized Late Triassic rocks.

The lower part of the sequence consists of a thick unit of basaltic lavas and tuffs. Upsection, they give way to tuffs and tuffites of mixed composition, which, in turn, are overlain by another basaltic unit. The overlying sedimentary sequence consists mainly of sedimentary rocks, sandstones, and gravelstones (rarely conglomerates) with rare tuff and tuffite interbeds. The volcanogenic–terrigenous sequence is overlain by a thick unit of platy limestones with Middle Permian fauna. A thick unit of felsic volcanic rocks ascribed according to [3] to the Upper Barabash Formation is located further southeast. The rocks are cut by dolerite, andesite, dacite, and rhyolite dikes. The general structural scheme of the sequence and the position of sampling points are shown in Fig. 2. The contacts between units of volcanic, pyroclastic, and sedimentary rocks are mainly overlain by Quaternary sediments and usually are inaccessible for direct observation.

METHODS

Petrographic study of the rocks was performed in standard polished thin sections. The contents of major components in the rocks were determined by the XRF method at the Analytical Center of the V.S. Sobolev Institute of Geology and Mineralogy of the Siberian Branch of the Russian Academy of Sciences (analysts N.M. Glukhova, N.G. Karmanova, and A.N. Taryanik) using the standard technique. The contents of trace and rare-earth elements were determined by inductively coupled plasma mass spectrometry (ICP-MS) at the Analytical Center of the V.S. Sobolev Institute of Geology and Mineralogy of the Siberian

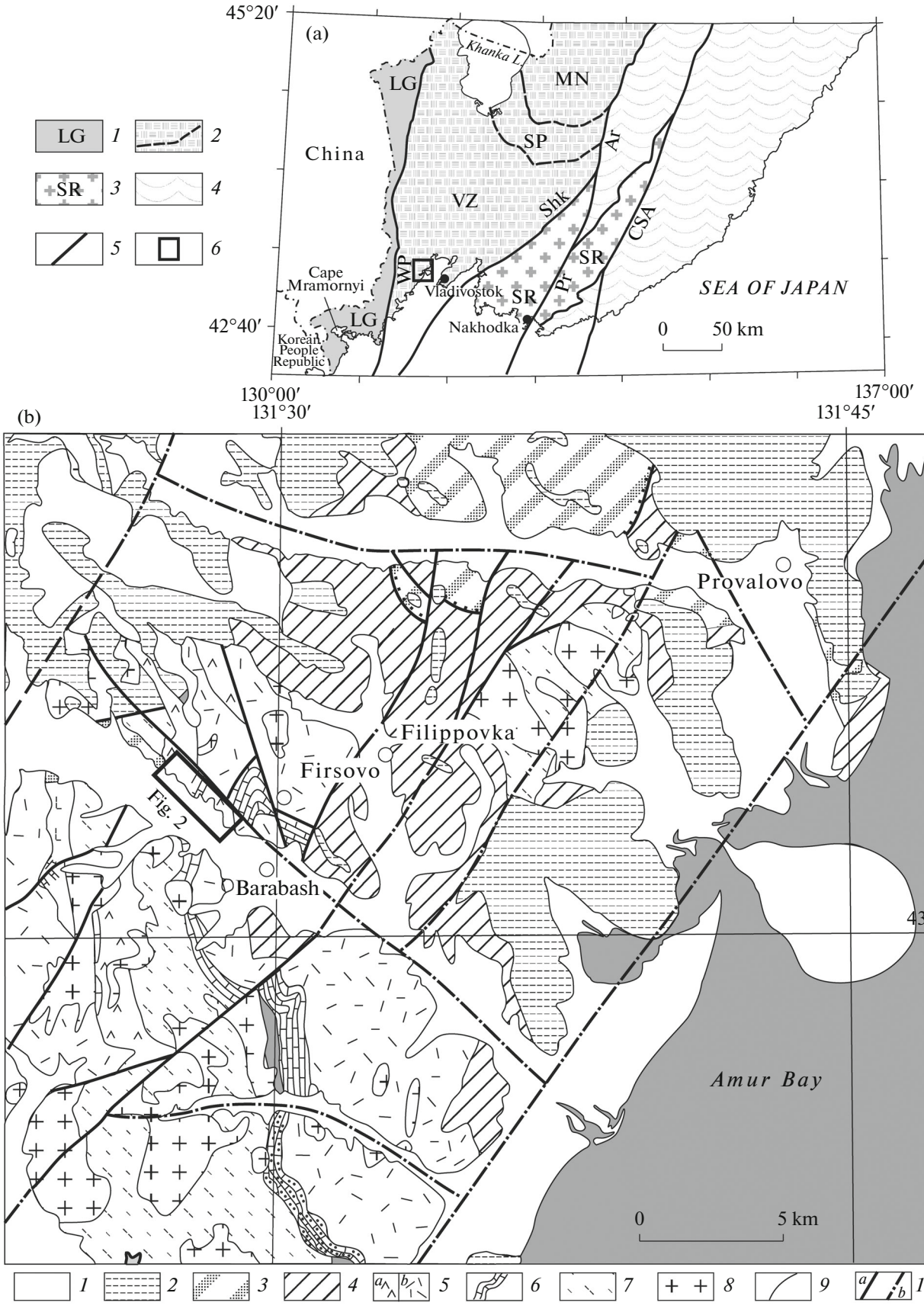
(a)
45°20′
42°40′
130°00′
131°30′
137°00′
131°45′
Khanka L.
LG
MN
SP
Ar
China
VZ
Shk
CSA
SR
WP
Cape Mramornyi
Vladivostok
Pr
SEA OF JAPAN
Nakhodka
Korean People Republic
0 50 km
LG 1
2
SR 3
4
5
6
(b)
Provalovo
Filippovka
Firsovo
Fig. 2
Barabash
43°10′
Amur Bay
0 5 km
1
2
3
4
5
6
7
8
9
10

Fig. 1. (a) Scheme of the terranes of South Primorye (after [2]). (*1*) Laoelin–Grodekov terrane—a fragment of the Late Paleozoic active margin; (*2*) terranes of the Early Paleozoic Bureya–Khanka orogenic belt: (MN) Matveevka–Nakhimovka, (SP) Spassk, (VZ) Voznesenka, and boundaries between them (dash); (*3*) Sergeevka terrane—fragment of the Paleozoic and Mesozoic passive margin, which is included in the structure of the Mesozoic orogenic belt; (*4*) terranes of the Late Mesozoic Sikhote Alin–North Sakhalin orogenic belt; (*5*) faults, including (WP) West Primorsky, (Shk) Shkotovsky, (Ar) Arsen'evsky, (Pr) Partizansky, (CSA) Central Sikhote Alin; (*6*) studied area. (b) Geological scheme of the southern Voznesenka terrane (mopdifed after [3]). (*1–4*) Mesozoic–Cenozoic deposits: (*1*) Quaternary; (*2*) Paleogene–Neogene; (*3*) Cretaceous; (*4*) Late Triassic; (*5–6*) rocks of the Barabash Formation: (*5*) subformation: (a) lower and (b) upper; (*6*) marker limestone horizons with Capitanian fauna; (*7*) volcanosedimentary sequences of the Vladivostok Formation (P_2); (*8*) Permian granitoids; (*9*) geological boundaries; (*10*) faults: (a) proved, (b) inferred.

Branch of the Russian Academy of Sciences (Novosibirsk) using a Finnigan Element (analysts I.V. Nikolaeva and S.V Palesskii). The procedures of sample preparation and analysis are given in detail in [10].

Accessory zircons were extracted by S.N. Rudnev at the V.S. Sobolev Institute of Geology and Mineralogy of the Siberian Branch of the Russian Academy of Sciences. U–Pb studies were conducted at the Far East Geological Institute of the Far East Branch of the Russian Academy of Sciences using an NWR-213 UV laser system (Electro Scientific Industries Inc., USA) coupled to an Agilent 7500a ICP-MS (Agilent Technologies Inc., USA) with a laser beam of 20 μm in size, ablation time of 100 s, and crater depth up to 30–40 μm. In general, the technique of analytical studies is close to that described in [13].

Zircon grains were implanted in epoxy and then were sequentially washed in a warm ultrasonic bath in 2% Citranox solution (Alconox Inc., USA) to remove possible impurities and in 2% HNO_3 to remove possible lead contamination. This procedure makes it possible to avoid "pre-ablation" of the studied sample.

The measurement technique of the isotope ratios is described in detail in [1, 8]. The mass spectrum was scanned over the centers of the following masses: 206, 207, 208, 232, and 238. No measurements were conducted for mass 204 because of the ubiquitously high Hg background in the spectrum. The U–Pb age was calculated using the GLITTER software [www.mq.ed.au/GEMOC]. The stability of the device operation and reproducibility were controlled by analyzing Temora 2 zircon standard (every eighth measurement). The concordia diagrams and error ellipses were plotted using the Isoplot/Ex v. 3.00 package [15].

PETROGRAPHIC CHARACTERISTICS OF THE ROCKS

The basalts from the lower part of the sequence represent black or dark gray finely porphyritic rocks. The phenocrysts (varying from single to 20–30% and reaching 5 mm in size) are practically completely replaced by large chlorite laths. There are rare clinopyroxene relicts, while some phenocrysts (judging from the morphology) represent replaced olivine grains. The hyalopilitic groundmass is made up of fine split oligoclase crystals, fine equant grains of ore mineral, and decomposed dark brown volcanic glass. The plagioclase frequently forms fan-shaped aggregates, which are replaced by carbonate with high relief and anomalous interference colors. The rocks have a fluidal, locally finely vesicular, structure, with pores filled by chlorite–carbonate material.

The *basalts of the upper unit* are dark gray porphyritic rocks. Phenocrysts up to 1 cm in size (amounting 45–50 vol %) are represented exclusively by elongated prismatic plagioclase. The crystals show clear zoning and broad twin bands. The groundmass has a microdoleritic texture, where the interstices between the "framework" of small plagioclase euhedral laths are filled with almost equant mafic mineral (clinopyroxene mainly replaced by chlorite or, more rarely, epidote) and small magnetite crystals. The rocks have a massive, locally finely vesicular, structure.

The *tuffs and tuffites* are usually greenish gray to light gray rocks. The tuffs are vitric–lithic. The rock fragments are dominated by glass and volcanic rocks of felsic composition (rhyolites), with less common plagioclase porphyrites and quartz porphyry. The glass fragments are identified by their shelly texture typical of volcanic glasses and have very low relief in transmitted light. It is seen under crossed nicols that they consist of fine plagioclase microlites and quartz grains. The felsic volcanics are porphyritic rocks with phenocrysts of finely twinned sodic plagioclase and quartz in an optically isotropic groundmass. The fragments of plagioclase porphyrites are frequently fused and subjected to greenstone alterations (the plagioclase and mafic minerals distinguished by morphology and relicts are practically completely replaced by chlorite and black ore minerals). The groundmass is made up of pumice, the pores of which are filled with chlorite and fine acicular plagioclase, usually sericitized and/or carbonatized.

The tuffites differ from the tuffs in their more rounded fragments and dark gray groundmass. The fragments, in addition to the above-described volcanic rocks and glass, are also represented by numerous (up to sharp predominance) quartz and feldspar grains.

The quartz, amounting to up to 70% of the clasts, is variably rounded (mainly weakly rounded, partially faceted) and frequently shows cloudy extinction. The plagioclase forms moderately rounded, nonzoned grains, frequently with fine twin hatching. The groundmass is made up of pelite-size particles, includ-

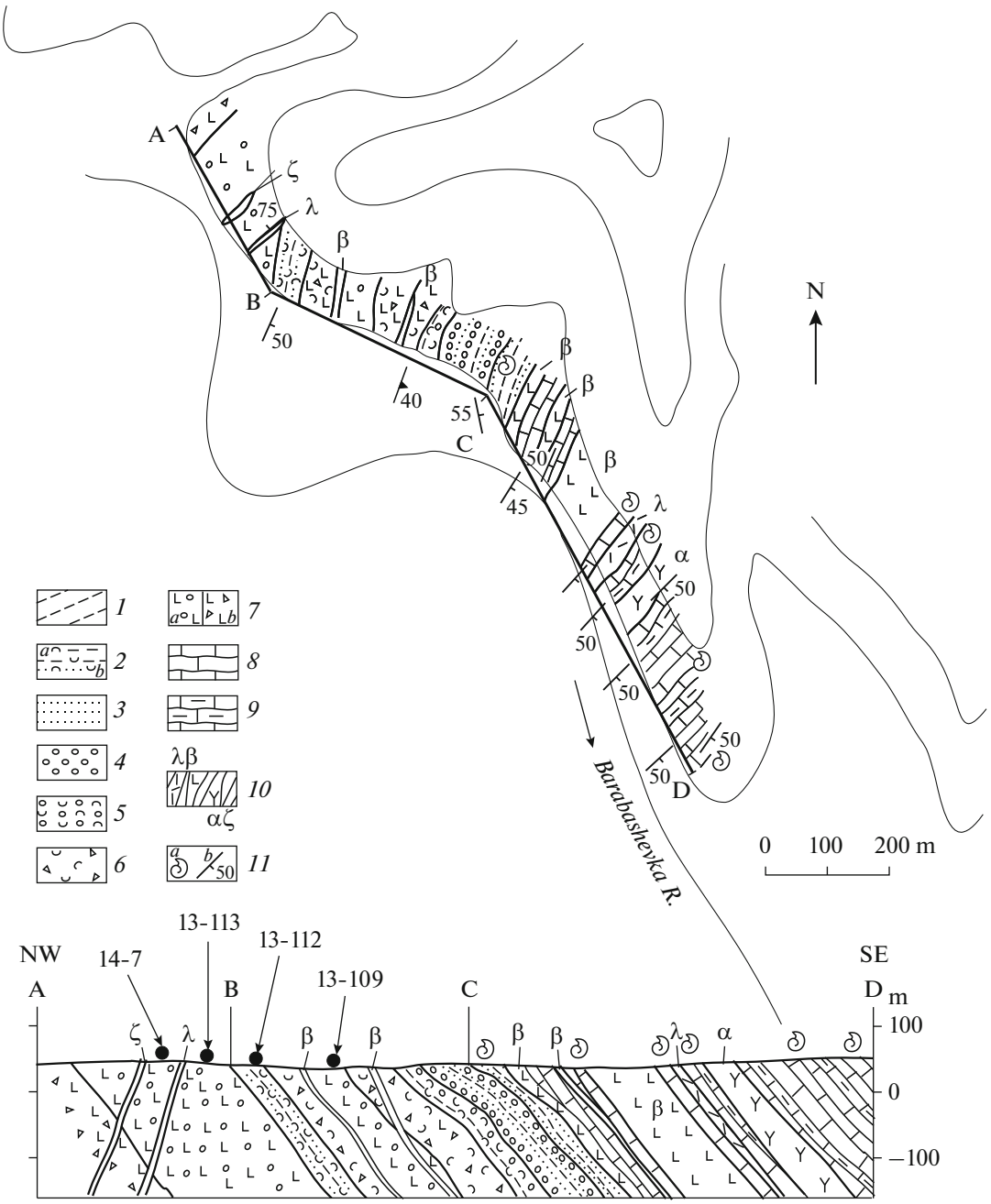

Fig. 2. Schematic section of the Middle Barabash subformation and sampling localities (arrows). Left bank of the Barabashevka River, 3 km upstream of Barabash settlement. (*1*) siltstones; (*2*) silty (a) and psammitic (b) tuffites; (*3*) sandstones; (*4*) conglomerates, gravelstones; (*5*) tuff conglomerates; (*6*) tuffs of mixed composition; (*7*) basalts and their tuffs (b); (*8*) limestones; (*9*) marls; (*10*) dikes of rhyolite (λ), basalt (β), andesite (α), and dacite (τ); (*11*) localities of microfauna finds (a), orientation of lamination (b).

ing fine fragments of magnetite, quartz, and feldspar no more than 0.03 mm in size.

The *sandstones* correspond to silty quartz graywackes with clayey–carbonate cement. The fragments are dominated by quartz and cherts, with single plagioclase grains and rock fragments.

The quartz, amounting to approximately 70–80% of the clastic part, frequently has cloudy extinction. The grain size varies from 0.009 to 0.16 mm, with the predominance of 0.07–0.05 mm grains. The grains are rounded to varying extents, with the predominance of weakly rounded partially faceted grains. The rock fragments (no more than 20–30% of the total clastic component) are usually rounded with depressions on their surface. The rocks are microquartzites, glassy felsic volcanic rocks, and tuffs. The clastic component has a

fine-grained texture. The cement accounts for no more than 20 vol % and has a clayey–quartz–carbonate composition. The cement is of the island, discontinuous contoured type, with regeneration, penetration, and locally replacement relations between the clasts. The microstructure is massive.

The limestones are gray and light gray pelitomorphic rocks, with abundant remains of crinoid stems and rare brachyopods. Individual units (up to a few m thick) have a finely platy structure: platelets up to 3–10 cm thick are separated by interbeds of dark gray marls (1–3 cm).

COMPOSITION OF BASALTS

The basalts from the lower part are characterized by low SiO_2 (45–49 wt %) at elevated TiO_2 (11.8–2.4 wt %) and P_2O_5(0.32–0.99 wt %) contents. The alkali contents show strong variations (Na_2O + K22O = 4.3–6.9 wt %, K_2O = 0.55–2.1 wt %). The data points fall in the field of rocks of normal and moderately alkaline series in the TAS diagram (Fig. 3a) and define a linear trend from subalkaline to alkali basalts in the Winchester and Floyd diagram (Fig. 3b). The rocks correspond to the middle- and high-potassium rocks in the SiO_2–K_2O diagram (Fig. 3c) and form a nonsystematic swarm around the tholeiitic differentiation trend in the Myashiro diagram (Fig. 3d). They are also characterized by elevated Al_2O_3 (15–20 wt %), low Mg# (20–47), and low Ca contents (Table 1).

The trace-element composition of the rocks is characterized by wide variations of incompatible trace elements. The HFSE and REE contents in the most depleted varieties (low-Ti and low-P rocks) are close to those of N-MORB (Zr 140–170 ppm, Hf 4–4.5 ppm, Y 29–32 ppm, Nb 4.5–5.0 ppm, Ta 0.25–0.3 ppm, Th 0.3–0.6 ppm, ΣREE 45–70 ppm, $(La/Yb)_N$ 0.7–1.0, Figs. 4a, 4b, Table 1). The REE, Zr, Hf, and Y contents in the most enriched varieties are close to those of OIB, whereas their Th, Nb, Ta, and Ti contents are much lower than the contents typical of this rock type, resembling more closely the E-MORB type (Table 1). All of the studied rocks are characterized by enrichment in large-ion lithophile elements (Rb and Ba). Sr shows a complex behavior: the spidergramms show a positive anomaly in the depleted varieties and a negative anomaly in the most enriched varieties (Fig. 4b). Such variations in the alkali and alkali earth metals are likely caused by postmagmatic alteration of the rocks, rather than by the specifics of crystallization differentiation. This, in particular, is supported by the distinct correlation between Sr and Eu accumulating mainly in the plagioclase (Fig. 4b).

In general, the basalts from the lower part of the sequence in terms of the geochemical composition are confidently identified as oceanic rocks (rocks of spreading centers and oceanic islands). This is confirmed by the position of the data points in the discriminant diagrams (Figs. 5a, 5b).

The basalts from the upper unit sharply differ in composition from the described basalts of the lower unit (Table 1). They are characterized by the higher SiO_2 content, lower TiO_2 and P_2O_5 (1.3–1.4 and 0.28–0.33 wt %, respectively), lower contents of FeO and MgO, and elevated CaO (Table 1) content. The alkali contents in them show more narrow variations than those in the basalts from the lower part of the sequence (Na_2O + K_2O = 4–6.1 wt %, K_2O = 1.1–1.7 wt %). The data points of the rocks fall on the boundary between the fields of normal and elevated alkalinity in the TAS diagram (Fig. 3a) and are plotted in the field of high-potassium rocks in the SiO_2–K_2O diagram. However, the position of the data points in the Winchester–Floyd diagram (applied to avoid the effect of spilitization on the composition of the volcanic rocks) indicates their affiliation to the series of normal alkalinity (Fig. 3b).

The trace element composition is characterized by slightly lowered concentrations of high-field-strength elements as compared to the basalts from the base of the sequence (90–100 ppm Zr, 22–24 ppm Y, 2.7–3 ppm Hf, 4.8–5.4 ppm Nb, ~0.3 ppm Ta) and much higher Th contents (2.6–3 ppm). The rocks have near-clarke REE contents (ΣREE 98–110 ppm). The REE patterns show an asymmetric distribution with $(La/Yb)_N$ = 4–5 and a subtle positive Eu anomaly (Fig. 4a). The spidergramms (Fig. 4b) show a clear negative Nb and Ta anomaly and a positive Sr anomaly.

In the discriminant diagrams (Fig. 5), the data points of the basalts from the upper subformation either fall in the fields of the volcanic-arc rocks or in the within-plate rocks, near the boundary with the island-arc rocks.

It should be noted that the basalts of the studied sequence (lower and upper parts) sharply differ in composition from the basalts of the Barabash Formation of the Laoelin–Grodekov terrane. Table 1 and Figs. 3–4 show the chemical compositions of the basalts from the lower subformation of the Barabash Formation from the sequence in the Cape Mramornyi area. As compared to the basalts from the sequence base along the Barabashevka River, these rocks have lower TiO_2 contents, lower K_2O and P_2O_5, and clearly expressed "suprasubduction" signatures. As compared to the basalts of the upper unit, they have elevated contents of FeO and MgO and lower contents of K_2O, P_2O_5, and practically all incompatible elements. At the same time, it should be noted that the two groups of basalts have similar shapes of the spidergramms (Fig. 4b). The rock groups have similar magnesium number and, hence, the observed differences cannot be considered as products of the different degree of melt differentiation and thus indirectly confirm their

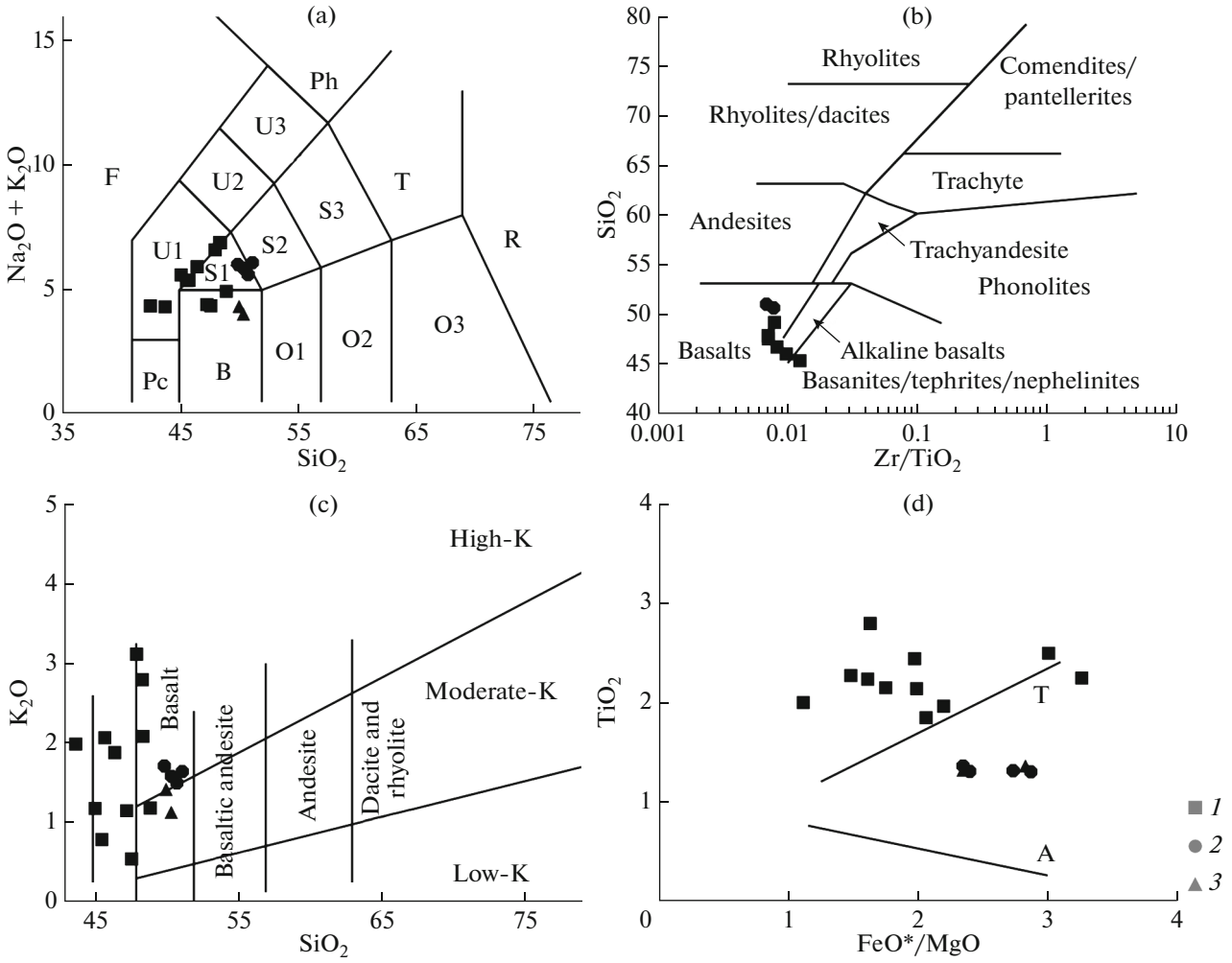

Fig. 3. Geochemical diagrams for basalts from section along the Barabashevka River. (a) SiO_2–alkali diagram [14]; fields: (F) foidolite, (Pc) picrobasalt, (B) basalt, (O1) basaltic andesite, (O_2) andesite, (O_3) dacite, (S1) trachybasalt, (S2) trachybasaltic andesite, (S3) trachyandesite, (T) trachyte, trachydacite, (R) rhyolite, (U1) tephrite, basanite, (U2) phonotephrite, (U3) tephrophonolite, (Ph) phonolite. (b) Zr/TiO_2–SiO_2 diagram [20]. (c) SiO_2–K_2O diagram, boundaries between fields after [18]. (d) FeO*/MgO–TiO_2 diagram [16]; trends T—tholeiitic, (A)—calc-alkaline. (*1*) basalts from the lower part, (*2*) basalts from the upper part, (*3*) basalts of the Barabash Formation of the Laoelin–Grodekov terrane (sequence in the Cape Mramornyi area).

affiliation to a single stage of magmatic activity. In our opinion, this indicates that the basalts were derived from a similar source. On the basis of their geochemical characteristics, this source was lithospheric mantle reworked by subduction processes. In this respect, they sharply differ from the basalts from the lower part of the sequence along the Barabashevka River, whose geochemical characteristics point to derivation through melting of oceanic lithospheric mantle or asthenosphere.

AGE OF THE ROCKS

As was shown above, the faunal assemblage found in the limestones indicates that the rocks of the Barabash Formation in the Laoelin–Grodekov terrane were formed at the Capitanian stage (Middle Permian). However, the presence of sedimentary rocks formed in different facies conditions and basalts of different nature in the same sequence calls into question the extension of the age estimates obtained for the limestones to all of the rocks of the sequence.

To solve this question, we attempted to extract zircons from the tuffs and tuffites from the middle part of the sequence.

Zircon was extracted using the heavy liquid technique at the V.S. Sobolev Institute of Geology and Mineralogy of the Siberian Branch of the Russian Academy of Sciences (Novosibirsk). Only three zircon grains were extracted from a 2.5-kg sample of dacitic tuff (sample no. 14-7). The tuffite (sample no. 13-112) yielded around 50 grains, which then were used for U–Pb isotope dating. In total, we performed 28 isotope determinations on 25 grains (Fig. 6a). Except for three analytical points with high (over 10%)

Table 1. Representative analysis of basalts(1–8) sequence along the Barabashevka River: (1–6) basalts from the lower unit, (7–8) basalts from the upper unit; (9–11) sequence in the Cape Mramornyi area, basalts of the lower subformation. Fe_2O_3*—total iron as Fe_2O_3.

Sample no.	13-113/2	13-113/3	13-113/6	14-7/2	14-7/3	14-7/4	13-109/1	13-109/4	15-7/1	15-7/2	15-8/2
Element	1	2	3	4	5	6	7	8	9	10	11
SiO_2	45.18	47.72	47.37	45.85	49.02	46.55	50.48	50.86	49.10	51.82	50.98
TiO_2	2.37	2.13	2.14	1.84	1.99	2.43	1.30	1.31	1.00	1.03	1.08
Al_2O_3	15.00	19.14	17.66	18.79	16.46	19.47	19.42	19.4	17.72	14.99	16.87
Fe_2O_3*	19.26	12.89	11.70	13.01	8.68	11.81	9.48	9.5	10.39	11.43	10.52
MnO	0.17	0.25	0.24	0.11	0.13	0.1	0.14	0.16	0.17	0.17	0.15
MgO	4.09	5.83	6.02	5.68	7.02	5.38	2.97	3.13	6	4.45	6.99
CaO	6.11	4.11	8.12	5.79	8.41	4.06	6.91	7.34	10.81	7.66	7.75
Na_2O	4.42	3.82	3.26	3.31	3.76	4.05	4.28	4.11	2.49	4.01	3.54
K_2O	1.19	0.55	1.16	2.07	1.19	1.89	1.59	1.51	0.9	1.06	0.81
P_2O_5	0.99	0.32	0.42	0.38	0.48	0.47	0.28	0.28	0.11	0.15	0.19
L.O.I.	1.41	3.52	2.01	3.28	2.72	3.81	2.62	2.38	1.16	2.58	1.36
Total	100.21	100.28	100.09	100.35	100.05	100.37	99.48	99.98	99.97	99.46	100.35
Sc	29.3	29.6	31.4	31.4	31.2	36.6	23.8	22.7	35.8	39.8	41.2
Co	10.4	13.2	40.4	20.8	40.9	55.8	19.6	18.3	30.1	30.2	28.7
Ga	17.2	20.7	17.9	20.5	17.4	22.1	19.0	17.6	16.3	17.2	17.1
Rb	31	17	27	64	26	51	41	32	27	24	17
Sr	450	349	370	523	539	569	778	745	417	369	376
Y	55	31	53	31	35	34	25	23	18	21	21
Zr	290	148	150	177	155	198	100	88	47	55	75
Nb	13.4	4.8	4.3	5	4.2	5	5.4	4.9	1.5	1.9	2.4
Cs	2.6	8.4	6.6	8	2.9	7.4	12.5	6.9	6	1.6	2.3
Ba	425	210	389	1060	324	914	453	443	129	262	161
La	37.98	3.53	6.68	7.83	14.5	30.64	18.25	16.4	4.72	7.6	7.43
Ce	99.37	9.11	18.59	20.48	39.01	70.62	38.12	35.31	10.79	15.61	16.7
Pr	16.02	1.71	3.6	3.28	6.07	9.16	5.71	5.15	1.62	2.12	2.33
Nd	66.08	8.63	20.55	15.07	28.61	36.12	23.04	20.72	6.92	9.54	10.59
Sm	12.59	2.88	7.7	4.49	7.34	7.46	5	4.64	2.21	2.94	3.24
Eu	4.01	1.44	2.35	1.91	2.81	1.75	1.71	1.59	0.94	0.96	1.1
Gd	11.17	3.98	9.38	5.59	7.67	7.46	4.4	4.29	2.67	3.43	3.49
Tb	1.66	0.75	1.66	0.89	1.15	1.02	0.73	0.67	0.48	0.53	0.56
Dy	9.45	5.01	10.1	5.38	6.53	5.77	4.28	4.02	2.99	3.64	3.74
Ho	1.88	1.11	2	1.16	1.28	1.13	0.86	0.78	0.62	0.78	0.8
Er	5.40	3.18	5.7	3.31	3.60	3.4	2.45	2.25	1.9	2.2	2.22
Tm	0.81	0.49	0.8	0.48	0.52	0.5	0.38	0.35	0.29	0.36	0.35
Yb	5.10	3.13	4.96	3.15	3.38	3.18	2.5	2.14	1.93	2.4	2.3
Lu	0.75	0.46	0.75	0.48	0.51	0.49	0.37	0.32	0.29	0.36	0.35
Hf	7.5	4.2	4	4.5	4.1	5	3.1	2.7	1.4	1.7	2.1
Ta	0.7	0.3	0.3	0.3	0.3	0.3	0.3	0.3	0.1	0.1	0.1
Th	0.7	0.6	0.3	0.3	0.4	0.5	2.9	2.7	0.9	1.0	0.9
U	0.2	0.3	0.1	0.1	0.1	0.2	0.7	0.7	0.3	0.4	0.4

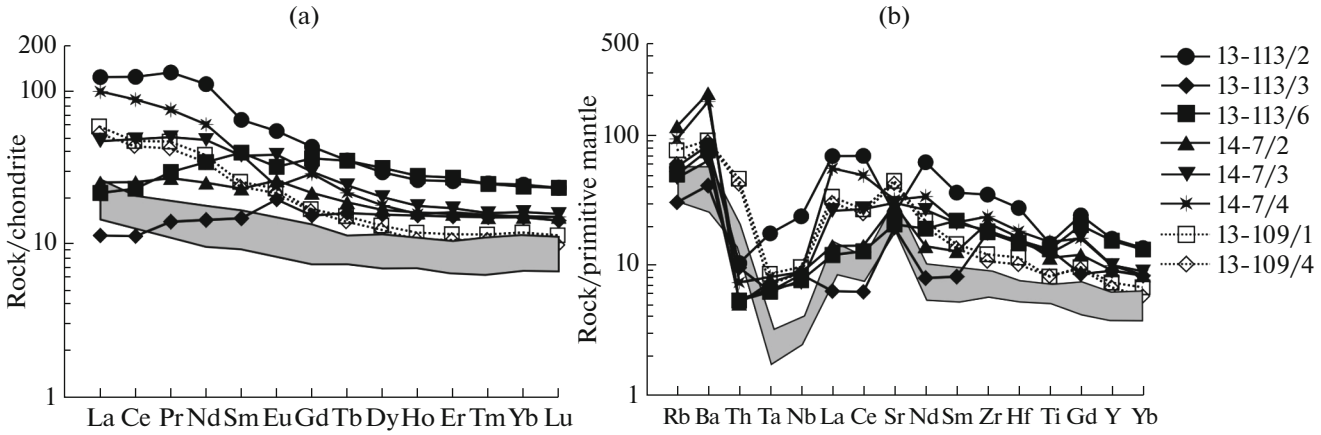

Fig. 4. REE (a) and multielement (b) distribution patterns for basalts from the section along the Barabashevka River. Sample numbers correspond to those in Table 1. Gray field shows the compositions of the basalts from the Mramornyi Cap sequence. REE abundances were normalized to chondrite after [12]; multielement diagrams are normalized to the primitive mantle after [19].

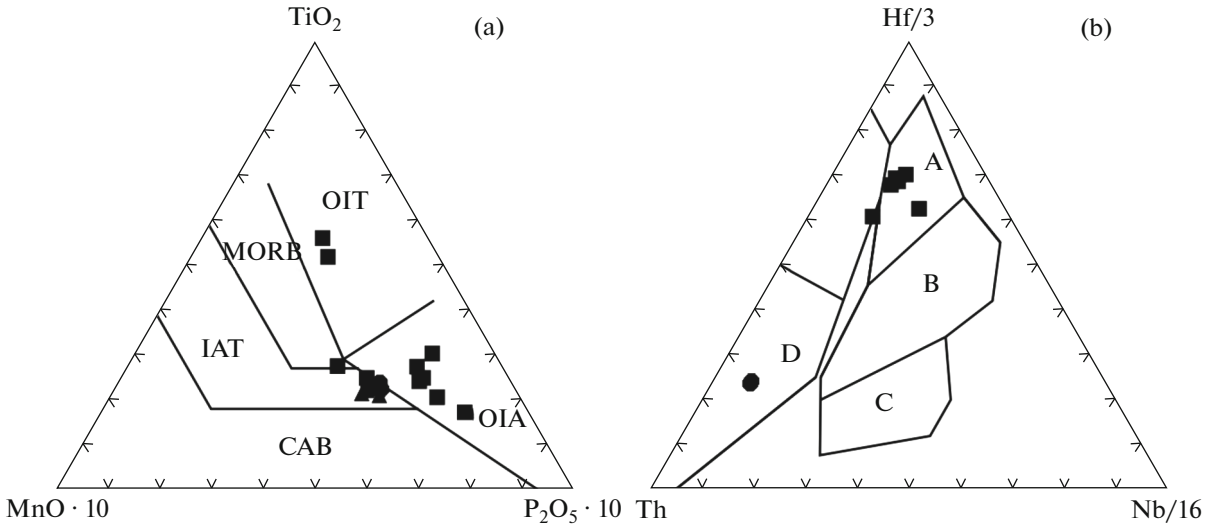

Fig. 5. Discrminant diagrams for basalts from the Barabashevka River sequence.(a) diagram MnO*10–TiO_2–P_2O_5*10 [16]; fields: (MORB) mid-ocean ridge basalts, (OIT) oceanic-island tholeiites, (OIA) oceanic island alkali basalts, (IAT) island arc tholeiites, (CAB) calc-alkaline basalts. (b) Th–Hf/3–Nb/16 diagram [21]; fields: (A) N-MORB; (B) E-MORB, within–plate tholeiitic basalts and their derivatives; (C) alkaline within-plate basalts and their derivatives; (D) volcanic arc basalts and their derivatives. Symbols are shown in Fig. 3.

discordance, all of the $^{206}Pb/^{238}U$ determinations are subdivided into five groups. One grain yielded a Precambrian age (740 ± 17 Ma); four points (three grains) showed Ordovician ages (476–461 Ma); seven points (six grains) showed Carboniferous ages (351–326 Ma); the most numerous zircon population (nine grains, ten analytical points) showed Permian ages (279–258 Ma); and three grains showed Middle Triassic ages (235–231 Ma). The concordant age calculated for the young points (grains nos. 7, 11, 12, Table 2) is 233.3 ± 3.3 Ma (MSWD = 0.89), which corresponds to the Ladinian Stage of the Middle Triassic (Fig. 6b).

The study showed that the zircon grains of different ages differ in morphology and internal structure. In particular, the Middle Triassic zircons (235–231 Ma) have euhedral shape, smoothed facets and faces, prismatic habitus (130–170 μm, K_{el} = 1.6–2.0), and oscillatory (magmatic) type of inner zoning (Fig. 7a). Their inner parts sometimes contain opaque ore minerals. The most numerous zircon population of the Permian age (279–258 Ma) is represented by both intact crystals and their fragments, which, judging from their morphology, have short prismatic habitus and subeuhedral shape, with oval facets and faces (Fig. 7b). The grain size varies from 125 to 190 μm (K_{el} = 1.5–2.0). As seen from the cathodoluminescent images, their internal structure is characterized by thin mag-

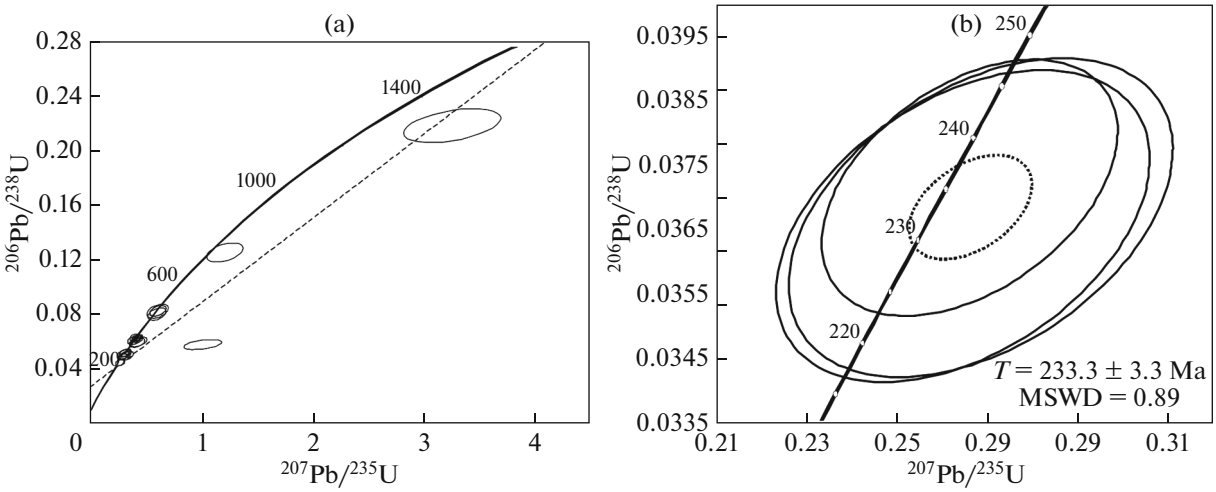

Fig. 6. U–Pb concordia diagram for zircons from tuffite sample 13-112. (a) all analyzed points; (b) three points of Triassic zircons.

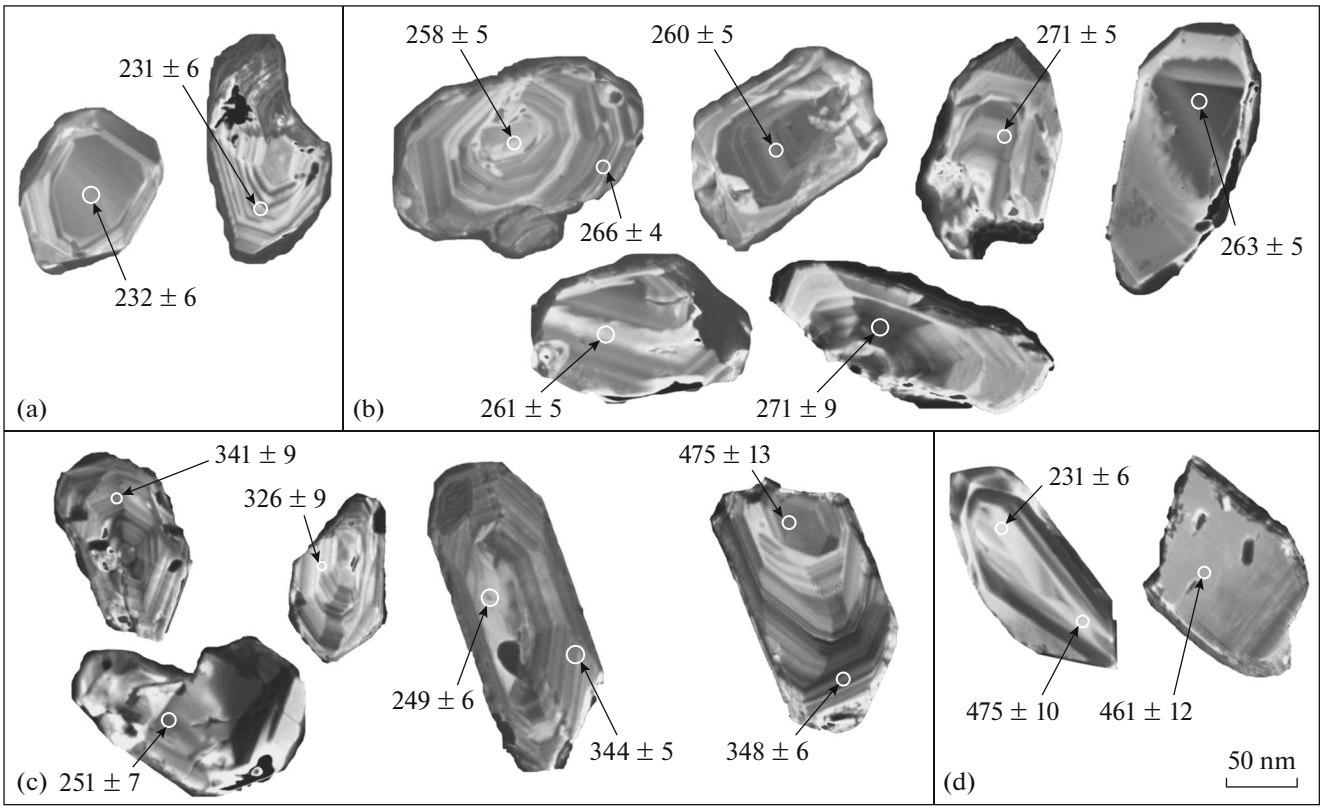

Fig. 7. Cathodoluminescent images of zircons from sample 13-112. (a) Triassic, (b) Permian, (c) Carboniferous, (d) Ordovician. See text for explanation.

matic zoning and by the presence of syngenetic transparent and opaque inclusions.

Individual zircon grains reveal signs of metamictization, local recrystallization, and dissolution, with the development of wide zones of zoned zircon of the late generation along their periphery.

The Carboniferous zircons (351–326 Ma) have prismatic habitus (120–300 μm, K_{el} = 1.8–2.7) and oval shape of facets and faces. They usually show oscillatory magmatic zoning and contain opaque syngenetic inclusions in the marginal and central parts of the crystals. Such inclusions are surrounded by a pleo-

Table 2. Results of single-grain zircon dating of tuffite sample 13-112 (section along the Barabashevka River)

Grain and point no	Isotope ratios		Rho	Ages ±1 σ (abs), Ma			D, %
	$^{207}Pb/^{235}U$ ±1σ %	$^{206}Pb/^{238}U$ ±1σ %		$^{207}Pb/^{206}Pb$	$^{207}Pb/^{235}U$	$^{206}Pb/^{238}U$	
1z	0.4257 ± 4.0	0.0557 ± 1.9	0.47	430 ± 91	360 ± 12	349 ± 6	3
1r	0.4097 ± 3.4	0.0549 ± 1.6	0.49	378 ± 77	349 ± 10	344 ± 5	1
2	0.2996 ± 2.8	0.0414 ± 1.5	0.53	306 ± 66	266 ± 7	262 ± 4	2
3z	0.2859 ± 4.7	0.0408 ± 2.0	0.43	233 ± 111	255 ± 11	258 ± 5	-1
3r	0.2957 ± 3.1	0.0421 ± 1.6	0.51	238 ± 73	263 ± 7	266 ± 4	-1
4z	0.6014 ± 6.4	0.0765 ± 2.8	0.44	492 ± 145	478 ± 25	475 ± 13	1
4r	0.4182 ± 4.1	0.0555 ± 1.9	0.47	399 ± 93	355 ± 12	348 ± 6	2
5	0.3167 ± 4.3	0.0429 ± 2.0	0.46	354 ± 100	279 ± 10	271 ± 5	3
6	0.2988 ± 4.0	0.0411 ± 1.9	0.47	318 ± 93	266 ± 9	260 ± 5	2
7	0.2658 ± 5.1	0.0372 ± 2.2	0.44	280 ± 118	239 ± 11	235 ± 5	2
8	0.4160 ± 4.2	0.0560 ± 2.0	0.47	364 ± 97	353 ± 13	351 ± 7	1
9	0.3030 ± 4.6	0.0416 ± 2.1	0.45	323 ± 107	269 ± 11	263 ± 5	2
10	0.2994 ± 4.3	0.0413 ± 2.0	0.46	312 ± 101	266 ± 10	261 ± 5	2
11	0.2682 ± 6.5	0.0367 ± 2.8	0.43	330 ± 150	241 ± 14	232 ± 6	4
12	0.2643 ± 6.4	0.0366 ± 2.7	0.43	305 ± 148	238 ± 14	231 ± 6	3
13z	0.6065 ± 4.9	0.0765 ± 2.2	0.46	510 ± 110	481 ± 19	475 ± 10	1
13r	0.6062 ± 4.8	0.0764 ± 2.2	0.46	511 ± 109	481 ± 19	475 ± 10	1
15	0.5958 ± 5.8	0.0741 ± 2.6	0.45	540 ± 131	475 ± 22	461 ± 12	3
16	0.4095 ± 6.5	0.0542 ± 2.7	0.42	402 ± 146	349 ± 19	341 ± 9	2
17	0.3168 ± 6.6	0.0442 ± 2.8	0.42	284 ± 154	279 ± 16	279 ± 8	0
18	0.3234 ± 6.4	0.0408 ± 2.8	0.44	508 ± 143	285 ± 16	258 ± 7	9
19	0.3250 ± 8.0	0.0420 ± 3.2	0.40	456 ± 178	286 ± 20	265 ± 8	7
20	*1.2107 ± 5.5*	*0.1217 ± 2.5*	*0.45*	*990 ± 115*	*806 ± 31*	*740 ± 17*	*11*
21	*3.2516 ± 5.5*	*0.2198 ± 2.4*	*0.44*	*1753 ± 103*	*1470 ± 43*	*1281 ± 28*	*13*
22	0.4206 ± 6.4	0.0519 ± 2.8	0.43	557 ± 142	357 ± 19	326 ± 9	8
23	0.3031 ± 8.5	0.0430 ± 3.4	0.41	247 ± 195	269 ± 20	271 ± 9	-1
24	*1.0104 ± 6.8*	*0.0502 ± 3.2*	*0.47*	*2300 ± 122*	*709 ± 35*	*316 ± 10*	*55*
25	0.4259 ± 7.7	0.0528 ± 3.2	0.42	549 ± 169	360 ± 23	332 ± 10	8

Sharply discordant determinations omitted from consideration are shown by italic type.

chroic halo. In addition, metamictization or recrystallization zones are sometimes developed along the grain periphery. Rarely, zircons of this age population have nearly equant shape (180 μm, K_{el} = 1.4) and clearly expressed resorbed and oval shapes of facets and faces. It is seen in the cathodoluminescence images (Fig. 7c) that the grains of such type have a spotty color with weak signs of oscillatory zoning and development of recrystallization and metamictization along their rims.

The ordovician zircons (475–461 Ma) found in the tuffites are morphologically diverse (Fig. 7d). One zircon type is prismatic (~175 μm, K_{el} = 2.3), subeuhedral, with oscillatory and sectorial internal zoning. Another type is observed as fragments of large crystals with oval facets and faces. This zircon bears signs of strong metamictization in the inner parts, is recrystallized along the periphery, and contains syngenetic inclusions of accessory minerals. In rare cases, the zircons of Ordovician age occur as xenogenic crystals in the inner parts of Carboniferous zircons. The xenogenic zircon is characterized by short-prismatic (~175 μm, K_{el} = 1.5) and subeuhedral shape and inner sectorial magmatic zoning.

DISCUSSION AND CONCLUSIONS

(1) Study of the age, morphology, and inner structure of the zircons from the tuffites has shown that they were derived from different sources: some grains are detrital (contained in the sedimentary matrix of the tuffite), while others were presumably entrained by magma passing through the continental crust, and only three grains mark the felsic explosive volcanism. The evidence for the Middle Triassic (no older) age of the pyroclastic sequences is the presence of zircons with traces of abrasion and later overgrowing in all older populations (including Permian). With allowance for the unconformable contact of the studied sequence with the overlying (Carnian) sediments of the Sadgorod Formation, its geological age cannot be significantly younger than the age of the youngest zircons in the tuffites (Ladinian stage). Thus, this indicates that some of the volcanic rocks of the studied area, which are presently ascribed to the Permian Barabash Formation, have Triassic age (the foremost, intermediate–acid volcanic rocks of the upper subformation). Correspondingly, it is highly possible that volcanism, subsequent orogenesis, and granite magmatism of this area occurred in the Triassic rather than in the Permian. This casts some doubt on the affiliation of the considered block to the Voznesenka terrane (as shown in Fig. 1), which remained "sterile" with respect to volcanic manifestations during the entire Triassic. Thus, it is more reasonable to include this block in the Laoelin–Grodekov terrane—the fragment of the Paleozoic active margin. In this case, it is required, first, to refine the position of the boundaries between these blocks, and, second, to revise the timing (toward younger ages) of the amalgamation of this block with the terranes of the Bureya–Khanka orogenic block.

(2) In the light of the obtained data, the studied "stratotype" sequence of the Barabash Formation is not a single stratigraphic sequence, but consists of tectonically juxtaposed rocks of different ages. In particular, the Middle Triassic felsic pyroclastic rocks have been identified as stratigraphically lower than the faunally characterized Middle Permian limestones. Correspondingly, some part of the boundaries shown in Fig 2 represents layerwise thrusts and the entire studied sequence may represent a fragment of an accretionary wedge in the structure of the Triassic active margin. This assumption is supported by the above-demonstrated juxtaposition of basalts from different sources.

The considered questions are of great importance for understanding the Late Paleozoic–Early Mesozoic geological history of Southern Primorye. Further structural, petrological–geochemical, and geochronological investigations of these rock complexes are required to confirm the obtained results. Determining the volume and nature of Triassic volcanism in the Laoelin–Grodekov terrane should be the subject of future studies.

ACKNOWLEDGMENTS

This work was supported by the Russian Foundation for Basic Research (project no. 13-05-006660).

REFERENCES

1. A. S. Vakh, O. V. Avchenko, V. I. Kiselev, S. A. Sergeev, and S. L. Presnyakov, "U–Pb isotopic geochronologic investigations of zircons from granites and ore-bearing metasomatites of the Berezitiovoe Gold–Polymetallic Deposit (Upper Amur Region)," Russ. J. Pac. Geol. **7** (6), 384–402 (2013).
2. *Geodynamics, Magmatism, and Metallogeny of East Russia*, Ed. by A. I. Khanchuk (Dal'nauka, Vladivostok, 2006) [in Russian].
3. *State Geological Map of the Russian Federation on a Scale 1: 200 000. Khanka Series. Sheets K-52-XII (Vladivostok), K-52-XVIII (Zarubino)* (VSEGEI, St. Petersburg, 2004) [in Russian].
4. *State Geological Map of the Russian Federation on Scale 1 : 1000000, Khanka Series. Sheets L-52 (Pogranichnyi), L-53 (oz. Khanka), K-52 (Vladivostok), and K-53 (Nakhodka)* (VSEGEI, St. Petersburg, 2006) [in Russian].
5. S. V. Kovalenko, "Continental Late Triassic volcanic rocks of southern Primorye," in *Correlation of the Far East and East Transbaikalian Mesozoic Continental Complexes. Proceedings of Stratigraphic Conference of the Far East RISC* (Chita, 2000), pp. 71–73 [in Russian].
6. N. N. Kruk, V. V. Golozubov, S. A. Kasatkin, S. N. Rudnev, A. A. Vrzhosek, M. L. Kuibida, and G. M. Vovna, "Granitoids of the Gamov Intrusion (southern Primorye): its peculiarities and indicator and geodynamic role," Russ. Geol. Geophys. **56** (12), 2134–2152 (2015).
7. N. N. Kruk, V. V. Golozubov, S. A. Kasatkin, and E. A. Kruk, "Permian volcanic rocks of the South Western Primorye: composition and possible tectonic interpretation," in *Geodynamic Evolution of the Central Asian Mobile Belt (from Ocean to Continent): Proceedings of Conference, Irkutsk, Russia, 2015* (IZK SO RAN, Irkutsk, 2015), vol. 13, pp. 127–129 [in Russian].
8. A. V. Maslov, G. M. Vovna, V. I. Kiselev, Yu. L. Ronkin, M. T. Krupenin, "U–Pb systematics of detrital zircons from the Serebryanka Group of the Central Urals," Lithol. Miner. Resour. **47** (2), 160–176 (2012).
9. G. B. Levashev, *Geochemistry of Paragenic Magmatites of Active Zones of Continental Margins* (DVO AN SSSR, Vladivostok, 1991) [in Russian].
10. I. V. Nikolaeva, S. V. Palesskii, O. A. Koz'menko, and G. N. Anoshin, "Analysis of geologic reference materials for REE and HFSE by inductively coupled plasma–mass spectrometry (ICP-MS)," Geochem. Int., **46** (10), 1016–1022 (2008).
11. L. M. Parfenov, N. A. Berzin, A. I. Khanchuk, G. Badarch, V. G. Belichenko, A. I. Bulgakov, S. I. Dril', G. L. Kirillova, M. I. Kuzmin, U. J. Nokle-

berg, Prokop'ev A.V., Timofeev V.F., Tomurtogoo O., and X. Yan', "A formation model of orogenic belts of Central and Northeastern Asia," Tikhookean. Geol. **22** (6), 7–41 (2003).

12. W. V. Boynton, *Cosmochemistry of the rare earth elements: meteorite studies*, in *Rare Earth Element Geochemistry*, (Elsevier, Amsterdam, 1984), pp. 63—114.
13. S. E. Jackson, N. J. Pearson, W. L. Griffin, and T. A. Belousova, "The application of laser ablation-inductively coupled plasma-mass spectrometry to in situ U/Pb zircon geochronology," Chem. Geol. **211**, 47–69 (2004).
14. R. W. Le Maitre, *A Classification of Igneous Rocks and Glossary of Terms: Recommendations of the International Union of Geological Sciences, Subcommission on the Systematics of Igneous Rocks* (Blackwell, Oxford, 1989).
15. K. R. Ludwig, "Isoplot 3.00—a geochronological toolkit for Microsoft Excel," Berkeley Geochronol. Center. Spec. Publ, No. 4 (2003).
16. A. Miyashiro, "Volcanic rock series in island arcs and active continental margins," Am. J. Sci. **274**, 321–355 (1974).
17. E. D. Mullen, "$MnO/TiO_2/P_2O_5$: a minor element discriminant for basaltic rocks of oceanic environments and its implications for petrogenesis," Earth Planet. Sci. Lett. **62**, 53–62 (1983).
18. P. C. Rickwood, "Boundary lines within petrologic diagrams which use oxides of major and minor elements," Lithos **22**, 247–263 (1989).
19. Taylor, S.R. and McLennan, S.M., *The Continental Crust: Its Composition and Evolution* (Blackwell, London, 1985).
20. J. A. Winchester and P. A. Floyd, "Geochemical discrimination of different magma series and their differentiation products using immobile elements," Chem. Geol. **20**, 325–343 (1977).
21. D. A. Wood, "The application of a Th–Hf–Ta diagram to problems of tectonomagmatic classification and to establishing the nature of crustal contamination of basaltic lavas of the British Tertiary Volcanic Province," Earth Planet. Sci. Lett. **50**, 11–30 (1980).

Recommended for publishing by G.L. Kirillova
Translated by M. Bogina